Si and Mg pair-doped interlayers for improving performance of AlGaN/GaN heterostructure field effect transistors grown on Si substrate*

Ni Yi-Qiang(倪毅强), He Zhi-Yuan(贺致远), Yao Yao(姚 尧),
Yang Fan(杨 帆), Zhou De-Qiu(周德秋), Zhou Gui-Lin(周桂林), Shen Zhen(沈 震),
Zhong Jian(钟 健), Zheng Yue(郑 越), Zhang Bai-Jun(张佰君), and Liu Yang(刘 扬)†

School of Physics and Engineering, State Key Laboratory of Optoelectronic Materials and Technologies, Sun Yat-Sen University, Guangzhou 510275, *China*

(Received 9 October 2014; revised manuscript received 24 December 2014; published online 27 March 2015)

We report a novel structure of AlGaN/GaN heterostructure field effect transistors (HFETs) with a Si and Mg pair-doped interlayer grown on Si substrate. By optimizing the doping concentrations of the pair-doped interlayers, the mobility of 2DEG increases by twice for the conventional structure under 5 K due to the improved crystalline quality of the conduction channel. The proposed HFET shows a four orders lower off-state leakage current, resulting in a much higher on/off ratio ($\sim 10^9$). Further temperature-dependent performance of Schottky diodes revealed that the inhibition of shallow surface traps in proposed HFETs should be the main reason for the suppression of leakage current.

Keywords: heterostructure field effect transistor (HFET), GaN on Si, interlayers, high on/off ratio

PACS: 73.40.–c, 73.61.Ey, 81.15.Gh, 78.55.Cr **DOI:** 10.1088/1674-1056/24/5/057303

1. Introduction

AlGaN/GaN heterostructure field effect transistors (HFETs) grown on Si substrate by metal organic chemical vapor deposition (MOCVD) are very promising in commercial applications of RF power devices and high-power switch devices. This is attributed to advantages of the high two-dimensional electron gas (2DEG) density and the high breakdown field of GaN-based materials, combined with the low manufacturing cost of Si substrates. Semi-insulating or high-resistivity GaN (HR-GaN) is essential for AlGaN/GaN HFETs to decrease parallel conduction between drain and source and to ensure a good pinch-off of the channel. The unintentional doped HR-GaN buffer has been achieved by introducing higher edge-type dislocation to compensating the n-type background residual donor.[1–3] The off-state performance of HFETs fabricated on these HR-GaN buffer layers encountered a bottleneck for further leakage current reducing, due to the poor confinement of the 2DEG, which could cause a much more serious problem when the gate length (L_g) of HFET decreases for higher frequency operation of the transistors.[4,5] The introduction of back barrier structures beneath the 2DEG channel, such as the AlGaN/GaN/AlGaN double-heterostructure and Mg-doped GaN buffer layer,[6–8] have been proved to be a very effective way to enhance carrier confinement with much lower leakage current. However, both a thick AlGaN back barrier layer and Mg-doped GaN would easily result in poor crystal quality, degradating the 2DEG channel layer grown subsequently. In addition, thick and heavy Mg-doped GaN would cause a serious memory effect of Mg atoms.[9–11] Thus, the output current densities of the fabricated HFETs were deteriorated correspondingly.

Therefore, both good output and pinch-off properties were expected in the HFETs grown on Si substrate. Here, a novel HFET structure was proposed, in which a very thin Mg-doped GaN (Mg–GaN) and Si-doped GaN (Si–GaN) pair-doped interlayers are inserted (see Fig. 1(a)). The thin Mg–GaN grown here not only ensures lower leakage current, but also weakens the memory effect of Mg atoms. The Si–GaN interlayer is necessary for compensating for the excess Mg[12] due to the memory effect[13] and preventing the 2DEG from depleting. It has also been reported that both proper Si- and Mg-doped concentrations in GaN or AlGaN can improve the structural quality.[14–16] In this experiment, by optimizing the doping concentrations of the pair-doped interlayers, the off-state performance improved significantly without sacrificing the output characteristics. The correlation between the material characteristics and device performance provides insight understanding of the mechanisms that improve electrical characteristics in HFETs.

*Project supported by the National Natural Science Foundation of China (Grant Nos. 51177175 and 61274039), the National Basic Research Project of China (Grant Nos. 2010CB923200 and 2011CB301903), the Ph.D. Program Foundation of Ministry of Education of China (Grant No. 20110171110021), the International Sci. & Tech. Collaboration Program of China (Grant No. 2012DFG52260), the National High-tech R&D Program of China (Grant No. 2014AA032606), the Science and Technology Plan of Guangdong Province, China (Grant No. 2013B010401013), and the Opened Fund of the State Key Laboratory on Integrated Optoelectronics (Grant No. IOSKL2014KF17).

†Corresponding author. E-mail: liuy69@mail.sysu.edu.cn

© 2015 Chinese Physical Society and IOP Publishing Ltd

2. Experiment

A conventional undoped AlGaN/GaN HFET structure was grown as a reference (B_0 in Table 1) on Si(111) substrate by MOCVD, which consists of a 30-nm high-temperature AlN buffer layer, a 1.6-μm HR-GaN layer with insertion of two low temperature grown AlN interlayers for strain engineering,[17] and finally a 25-nm AlGaN barrier layer with ∼ 30% Al composition. The proposed HFET with the Mg–GaN and Si–GaN interlayers, which were inserted beneath the 40 nm GaN channel (see Fig. 1(a)), were grown under the same growth conditions with the conventional structure except for different dopant flow rates. In the proposed HFET, the doping level of both the Si and Mg-doped interlayer reduced simultaneously to keep the Cp_2Mg/SiH_4 ratio as a constant of 20. Here we introduced the relative doping concentration (RDC) to represent the doping level, in which RDC-0, RDC-1, RDC-2, and RDC-4 represented B_0, B_1, B_2, and B_4 from the undoped to the higher doping level, respectively. Meanwhile, HFET devices and Schottky diodes were also fabricated, in which the Ti/Al/Ni/Au were deposited for ohmic contact with electron-beam evaporation and annealed at 830 °C for 30 s in nitrogen ambient and the Ni/Au was deposited for Schottky contact. The *I*–*V* performance was measured by an Agilent B1505A. The HFETs discussed here are all in the same dimension with L_g, L_{gs}, L_{gd}, and W_g values of 3, 3, 5, and 100 μm, respectively.

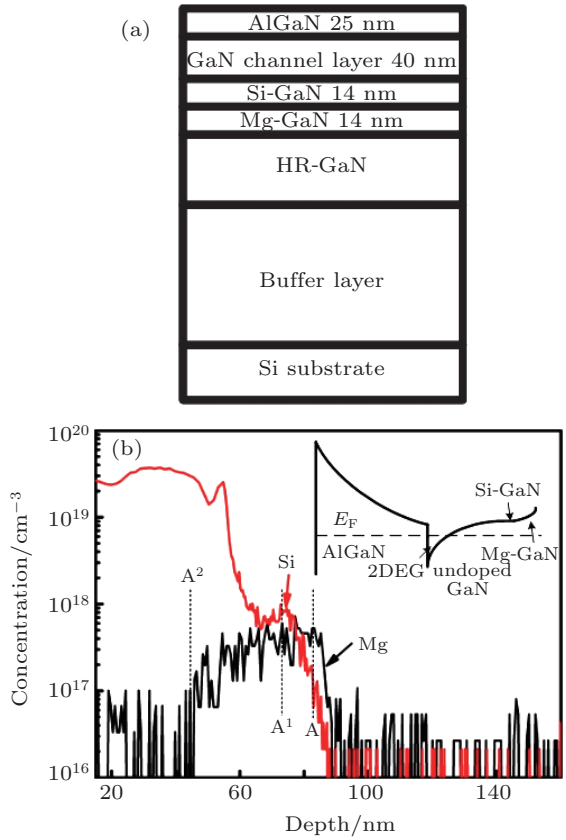


Fig. 1. (color online) (a) Schematic of AlGaN/GaN with Si and Mg pair-doped GaN interlayers. (b) SIMS profile of Si and Mg concentrations in sample B_1. Inset is the conduction band diagram for the proposed HFET structure.

3. Results and discussion

Figure 1(b) shows the secondary ion mass spectrometry (SIMS) profile of Mg and Si atoms concentration in sample B_1. The position mark A and A^1 indicate that the Cp_2Mg and SiH_4 sources were switched on, respectively. Due to the tiny Mg-doped concentration, the Mg profile delay tail (Mg memory effect) only extended about 30 nm (section AA^2 in Fig. 1(b)), which is 20 nm away from the 2DEG channel. While the higher Si signal in the initial stage (at the surface of the structure) of B_1 is affected by the surface Si pollution and the Silicon concentration for B_0 shows nearly the same level at the surface (SIMS data not shown here) which may be due to the contamination from the atmosphere after growth. The introduction of Si below the channel could effectively compensate for the excess Mg[12] due to the memory effect,[13] which made a Si and Mg co-doped interlayer exist here. In this co-doped region, the conduction band diagram of the proposed HFET is shown in the inset of Fig. 1(b). This increased barrier height is assumed to effectively prevent the leakage current through the buffer layer beneath the channel layer.

Table 1. Material characteristics and device properties of samples with various doping concentration levels.

	(Cp_2Mg/TMGa) /10^{-4} mol/mol	SiH_4/TMGa /10^{-5} mol/mol	Cp_2Mg/SiH_4 /mol/mol	RDC	XRD FWHM/arcsec		PL		Hall mobility/cm^2·V^{-1}·s^{-1}		AFM RMS	I_{Dmax}	R_{on}
					002	102	Peak/eV	FWHM/meV	300 K	5 K	@5 μm/nm	/mA·mm^{-1}	/Ω·mm
B_0	–	–	–	0	580	1090	3.401	41.8	1060	4095	0.56	718	5.6
B_1	1.5	0.75	20	1	602	1079	3.399	37.3	1200	7920	0.26	792	4.6
B_2	3	1.5	20	2	592	1093	3.397	41.9	985	5520	0.29	553	5.8
B_4	6	3	20	4	583	1113	3.379	100.7	539	1360	0.55	342	12

Room-temperature Hall measurement (Table 1) indicates that the conduction property improves with the RDC reducing from 4 to 1. The mobility of sample B_1 reaches 1200 cm^2/V·s, which is superior to that of undoped sample B_0. Furthermore, the temperature-dependent Hall effect measurements were carried out on these samples (see Fig. 2). The sheet carrier density of the investigated samples does not show any appreciable change (see Fig. 2(c)). The temperature-dependent electron Hall mobility in Fig. 2(a) shows that when the temperature drops to 5 K, the electron mobility of samples B_2 and B_1 reaches 5520 and 7920 cm^2/V·s respectively, which is significantly higher than that of a conventional sample

(4095 $cm^2/V{\cdot}s$). These phenomena indicate that the scattering becomes weak under lower temperatures. Several scattering mechanisms affect the electron mobility of 2DEG, and the separation of their contributions is usually performed through temperature-dependent measurement.[18–20] At high temperature (above 100 K), electron mobility decreases with increasing temperature, which is a typical temperature dependent of phonon scattering mobility. However, the low-temperature (below 100 K) electron mobility keeps almost the same, which is dominated by temperature-independent scattering factors, such as the interface roughness, alloy disorder, charged defect scattering and ionized impurity scattering. On one hand, in our experiments all the samples were grown under the same MOCVD condition except the different dopant flow rates in pair-doped interlayers. Therefore, the alloy disorder scattering effect should remain the same in all the investigated samples. On the other hand, a relatively low RDC (B_1) sample can lead to a growth condition with less charged defect scattering center, which can improve the mobility. Meanwhile, the sample with relative low RDC pair-doped interlayers and a 30 nm unintentionally doped GaN channel layer can minimize the influence of the ionized impurity scattering. However, the ionized impurity scattering can play a more important role on the reduction of the mobility in the relatively high RDC sample (B_4). The discussion above is the reason why the mobility varies from B_0 to B_4 as shown in Fig. 2(a). Furthermore, according to the well-known equation $\rho = 1/en\mu$ and the discussion above, we can easily understand why the sheet resistivity varies from B_0 to B_4 as shown in Fig. 2(b). All in all, the different doping level related channel crystal quality and interface roughness will be the key factors responsible for the improvement in electron mobility under low temperature.

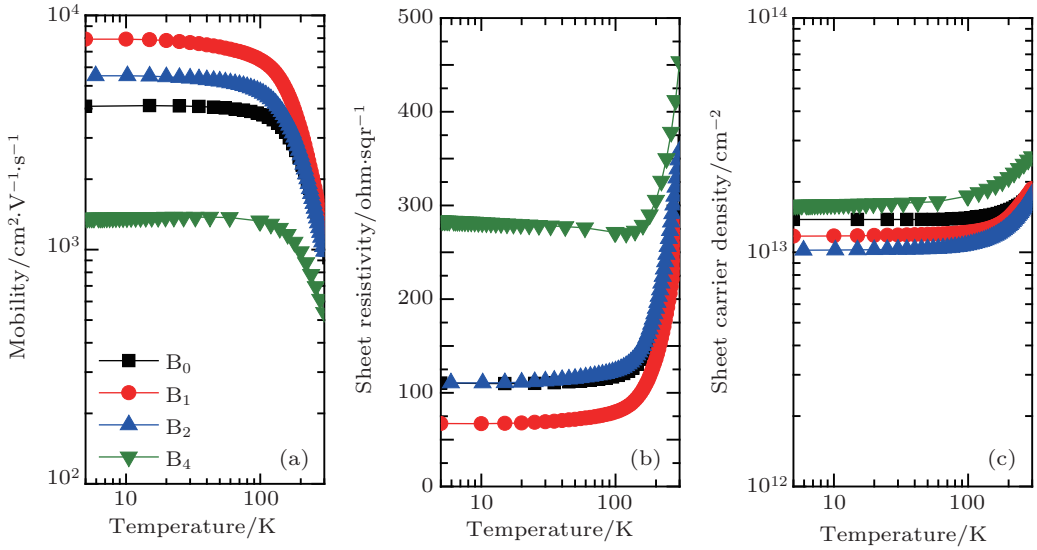


Fig. 2. (color online) (a) Hall effect mobility μ. (b) Sheet resistivity ρ and (c) sheet carrier density n versus temperature in log–log scale of the samples.

High-resolution x-ray diffraction (XRD) measurements were carried out to characterize the crystal quality and the influence of the Si/Mg interlayers on the strain state of the epilayer. As shown in Table 1, the FWHMs of (002) and (102) rocking curves of the investigated sample are all around 600 arcsec and 1100 arcsec, respectively, which is independent of the change of RDC. As we know, the detection depth of the XRD measurement can reach several hundred nanometers. This means that the FWHMs of (002) and (102) mainly reflect the crystal quality of the HR-GaN of the investigated samples, in which all the epilayers beneath the Si/Mg pair-doped interlayers in this work are grown in the same condition. Meanwhile, by measuring XRD reciprocal space maps (RSM) of the (105) reflections (not shown here), it is found that the AlGaN peaks of all the samples were perfectly aligned with the main GaN peak vertically, indicating that the insertion of the Si/Mg interlayers has no influence on the strain state of the AlGaN barrier layer and the GaN buffer layer. In order to evaluate the crystal quality around the channel, the room-temperature PL spectrum is recorded, which are very different from each other in Fig. 3, in which the topmost GaN layer mainly contributes to the luminescence. The spectra of all samples display intense band edge transition ($\sim$ 3.4 eV), while the I_{BE}/I_{BE0} intensity ratio (the band edge transition intensity for proposed samples to that of conventional sample B_0) increases significant by a factor of 4.3 in sample B_1. The highest luminescence intensity and best PL FWHM value of band edge transition (see Table 1) in sample B_1 is attributed to good suppression of non-radiative transitions, whose recombination rate is proportional to the density of native defects.[21] Therefore, in sample B_1

with the lowest Si and Mg dopant levels, the nonradiative related defects near the GaN channel layer reduce significantly in comparison with undoped or higher doped samples. Combining the PL with the Hall mobility results, a good correlation is observed with higher electron mobility as the band edge emission increases (see the inset in Fig. 3). It can be deduced that the quality of GaN near the 2DEG channel in the pair-doped interlayer improves with a lower density of defects, which may play an important role in the charged defect scattering.

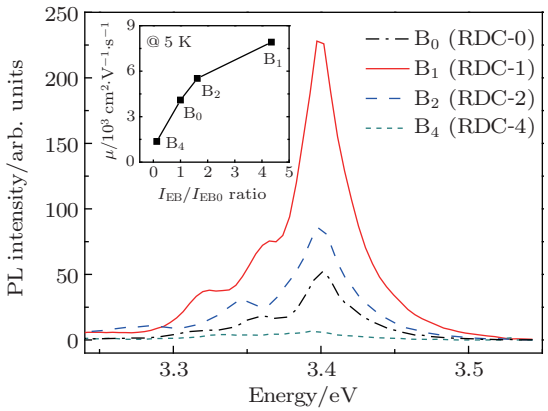


Fig. 3. (color online) Room-temperature photoluminescence spectrum. The inset shows the 2DEG mobility under 5 K against the ratio of the band edge intensity (I_{BE}/I_{BE0}) ratio.

In addition, it should be noted that the interface roughness would also be very sensitive to the Hall mobility of 2DEG. A clear step-flow growth surface is observed with all the samples, with the terrace width varying from 50 nm to 100 nm (not shown here). The surface root mean square (RMS) roughness values of these four samples are extracted and listed in Table 1, in which the sample B_1 has the smoothest surface with an RMS of 0.26 nm. This means the adsorption of Si or Mg atoms on the growth surface, which act as surfactants, appears to enhance the surface mobility of the group-III atoms. However, the increase of RMS value in sample B_4 with higher SiH_4 and Cp_2Mg flow rates may be ascribed to the increase of dislocation density.

The improvements in the conduction properties have also been verified by the HFETs device performance. The maximum drain current values I_{Dmax} and conduction resistance R_{on} were extracted from the output I–V properties and are shown in Table 1. When the doping concentration decreases, the output performance improves gradually and reaches the largest I_{Dmax} (792 mA/mm) in sample B_1, which increases by 10% in comparison with that of conventional sample B_0 (see Fig. 4(a)). Moreover, from the transfer characteristic (see Fig. 4(b)), it can be observed that the off-state channel leakage current was limited by the Schottky reverse leakage current in the gate region. The off-state drain leakage current density I_d reaches as low as 2.2×10^7 in sample B_1, which is about four orders lower in magnitude than that of B_0. This ultralow off-state channel leakage current, which is limited by the Schottky reverse leakage current, makes the current on/off ratio reach as high as 3.6×10^9 in sample B_1.

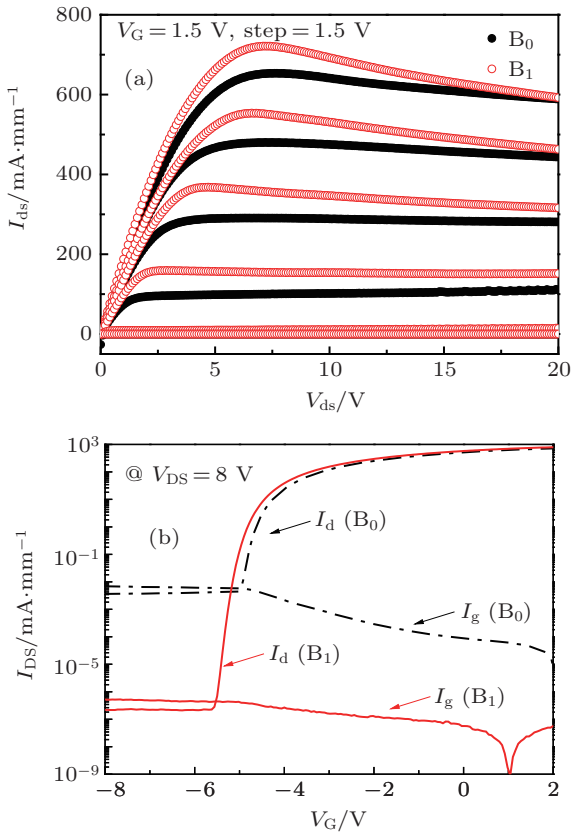


Fig. 4. (color online) (a) Output I–V properties and (b) semi-logarithmic transfer characteristic recorded at $V_{DS} = 8$ V for HFET fabricated on samples B_0 and B_1.

Therefore, in order to explore the mechanisms for the improvement in off-sate leakage current, Schottky diodes were also fabricated and characterized. Figure 5(a) shows the I–V characteristics of the Schottky diode in samples B_0 and B_1. The forward characteristic of B_1 is more ideal than that of B_0, due to the higher slope in the log-scale plot. Meanwhile, a much lower reverse leakage current is also observed in B_1 in comparison with B_0. Specifically, as shown in the inset of Fig. 5(a), we observe a linear dependence of $\ln(J/E)$ on $\sqrt{E}$ under the reverse-bias condition for both diodes, where J is the current density and E is the electric field in the semiconductor barrier. This indicates that the reverse leakage current is dominated by the Frenkel–Poole emission.[22] At room temperature, the carrier transport via conductive dislocations is the dominant source of reverse leakage currents in the Schottky contacts to the n-type nitride semiconductor material.[22–24] It is suggested that the key process in reverse leakage current flow is the emission of electrons from a trap state near the metal-semiconductor interface into a continuum state associated with the conductive dislocation.

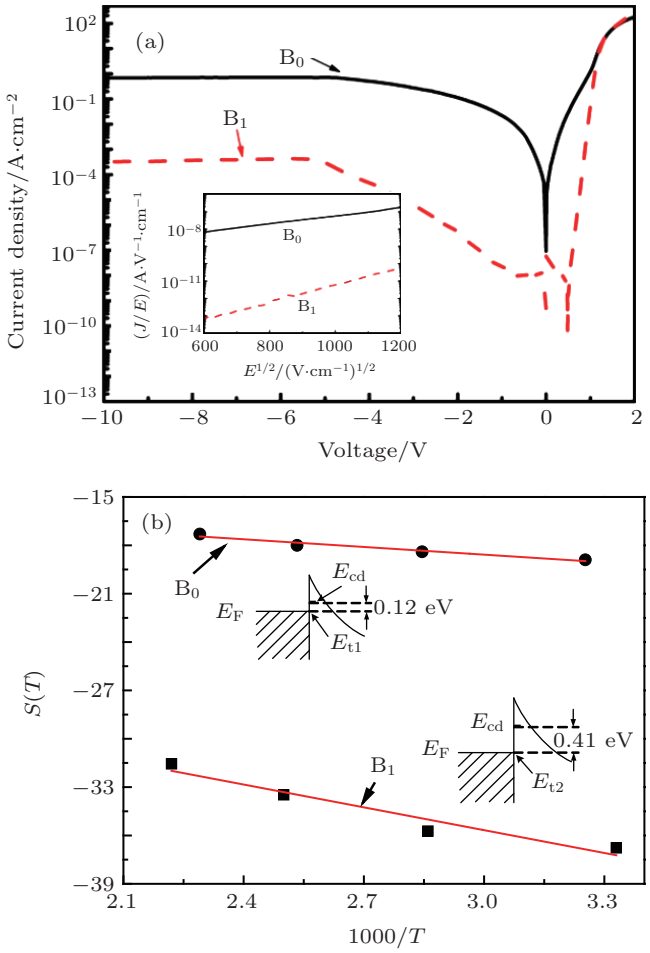


Fig. 5. (color online) (a) Comparison of the Schottky diode characteristics fabricated on samples B_0 and B_1. The inset shows the reverse-bias current density divided by an electric field versus the square root of the electric field. (b) Intercept $S(T)$ versus $1000/T$.

The current density associated with Frenkel–Pool emission is given by[22,25,26]

$$J = CE\exp\left[-\frac{q(\Phi_t - \sqrt{qE/\pi\varepsilon_0\varepsilon_s})}{kT}\right], \tag{1}$$

where Φ_t is the barrier height for the electron emission from the trapped state, ε_s is the relative dielectric permittivity, ε_0 is the permittivity of free space, T is the temperature, and k is Bolzmann's constant.

In Eq. (1), $\ln(J/E)$ should be a linear function of $\sqrt{E}$, i.e.,

$$\ln\left(\frac{J}{E}\right) = \frac{q}{kT}\sqrt{\frac{qE}{\pi\varepsilon_0\varepsilon_s}} - \frac{q\Phi_t}{kT} + \ln C$$
$$= R(T)\sqrt{E} + S(T), \tag{2}$$
$$R(T) = \frac{q}{kT}\sqrt{\frac{q}{\pi\varepsilon_0\varepsilon_s}}, \tag{3}$$
$$S(T) = -\frac{q\Phi_t}{kT} + \ln C. \tag{4}$$

As seen in the inset of Fig. 5(a), the leakage current densities are well described by the electric field dependence of Eq. (2).

Furthermore, the emission barrier height (Φ_t) values for the Schottky diode can be extracted from these data values. We measured the reverse leakage current from 300 K to 450 K. From the slope of $S(T)$ versus $1/T$ shown in Fig. 5(b), we obtain Φ_t values with 0.12 eV and 0.41 eV for samples B_0 and B_1, respectively. We assume that the trapped state (E_{t1} and E_{t2} for samples B_0 and B_1, respectively) should be close to the metal Fermi level[22] due to the pinning effect, as shown in both insets of Fig. 5(b). In both samples, the conductive dislocations (E_{cd}) are approximately in the same level of energy, as required for the conduction along dislocation lines across heterojunction interfaces. Thus, the relevant trapped state would be located 0.12 eV and 0.41 eV below the conductive dislocation level (E_{cd}) for samples B_0 and B_1, respectively. It is believed that the effective barrier height (Φ_{eff}) in the Schottky diodes of B_1 would also be much higher than that of B_0, which benefits from a higher emission barrier height. We speculated that the inhibition of shallow surface traps should be the main reason for the good suppression of reverse leakage current in sample B_1. This phenomenon is also consistent with the PL results, which confirms that the trap densities and surface states would seriously affect the device performance.

4. Conclusions

In summary, we have realized a novel HFET with Si and Mg pair-doped interlayers under the 2DEG conduction channel. From the analysis mentioned above, a pretty good correlation between the Hall electron mobility, PL intensity, and surface roughness was obtained. These Si and Mg pair-doped interlayers with lower doping concentrations enhance the 2DEG conduction performance with a lower density of defects and smoother surface roughness. In the proposed HFET, much higher current on/off ratio of $\sim 10^9$ are measured in comparison with an undoped sample, which benefits from the ultralow off-state leakage current. Further, the temperature-dependent leakage current performance of Schottky diodes indicates that the inhibition of the shallow surface traps should be the main reason for the good suppression of reverse leakage current in the proposed structure.

References

[1] Grzegorczyk A P, Hageman P R, Weyher J L and Larsen P K 2005 *J. Cryst. Growth* **283** 72
[2] Lu L, Shen B, Xu F J, Gao B, Huang S, Miao Z L, Qin Z X, Yang Z J, Zhang G Y, Zhang X P, Xu J and Yu D P 2008 *J. Appl. Phys.* **103** 113510
[3] Selvaraj J, Selvaraj S L and Egawa T 2009 *Jpn J. Appl. Phys.* **48** 121002
[4] Palacios T, Chakraborty A, Heikman S, Keller S, Denbaars S P and Mishra U K 2006 *Electron Dev. Lett. IEEE* **27** 13
[5] Lee D S, Gao X, Guo S, Kopp D, Fay P and Palacios T 2011 *Electron Dev. Lett. IEEE* **32** 1525
[6] Chang S, Wei S, Su Y, Liu C, Chen S, Liaw U, Tsai T and Hsu T 2003 *Jpn J. Appl. Phys.* **42** 3316
[7] Su Y K, Chang S J, Kuan T M, Ko C H, Webb J B, Lan W H, Cherng Y T and Chen S C 2004 *Mater. Sci. Eng. B* **110** 172

[8] Lee H, Hyun S, Cho H, Ostermaier C, Kim K, Ahn S, Na K, Ha J, Kwon D, Hahn C, Hahm S, Choi H and Lee J 2008 *Jpn J. Appl. Phys.* **47** 2824
[9] Ohba Y and Hatano A 1994 *J Cryst. Growth* **145** 214
[10] Chang Y, Ludowise M, Lefforge D and Perez B 1999 *Appl. Phys. Lett.* **74** 688
[11] Ran J, Wang X, Hu G, Wang J, Li J, Wang C, Zeng Y and Li J 2006 *Microelectron. J.* **37** 583
[12] Leem J, Lee C, Lee J, Kyu Noh S, Kwon Y, Ryu Y and Sung-Jin S 1998 *J. Cryst. Growth* **193** 491
[13] Ohba Y and Hatano A 1994 *J. Cryst. Growth* **145** 214
[14] Keller S, Chichibu S F, Minsky M S, Hu E, Mishra U K and Denbaars S P 1998 *J. Cryst. Growth* **195** 258
[15] Cho H K, Lee J Y, Kim K S and Yang G M 2001 *Solid-State Electron.* **45** 2023
[16] Cho H K, Lee J Y, Jeon S R and Yang G M 2001 *J. Cryst. Growth* **233** 667
[17] Ni Y Q, He Z Y, Zhong J, Yao Y, Yang Fan, Xiang P, Zhang B J and Liu Y 2013 *Chin. Phys. B* **22** 088104
[18] Shur M, Gelmont B and Asif Khan M 1996 *J. Electron. Mater.* **25** 777
[19] Gurusinghe M N, Davidsson S K and Andersson T G 2005 *Phys. Rev. B* **72** 45316
[20] Lisesivdin S B, Acar S, Kasap M, Ozcelik S, Gokden S and Ozbay E 2007 *Semicond. Sci. Technol.* **22** 543
[21] Reshchikov M A and Morkoç H 2005 *J. Appl. Phys.* **97** 061301
[22] Zhang H, Miller E J and Yu E T 2006 *J. Appl. Phys.* **99** 023703
[23] Miller E J, Schaadt D M, Yu E T, Poblenz C, Elsass C and Speck J S 2002 *J. Appl. Phys.* **91** 9821
[24] Hsu J W P, Manfra M J, Lang D V, Richter S, Chu S N G, Sergent A M, Kleiman R N, Pfeiffer L N and Molnar R J 2001 *Appl. Phys. Lett.* **78** 1685
[25] Yeargan J R and Taylor H L 1968 *J. Appl. Phys.* **39** 5600
[26] Chaneliere C, Autran J L, Four S, Devine R A B and Balland B 1999 *J. Non-Crystal. Solid.* **245** 73